Segment diffusion and nuclear magnetic resonance spin-lattice relaxation of polymer chains confined in tubes: Analytical treatment and Monte Carlo simulation of the crossover from...

ARTICLE *in* THE JOURNAL OF CHEMICAL PHYSICS · MARCH 2002

Impact Factor: 2.95 · DOI: 10.1063/1.1451242

4 AUTHORS, INCLUDING:

Nail Fatkullin
Kazan (Volga Region) Federal University
90 PUBLICATIONS **1,053** CITATIONS

Segment diffusion and nuclear magnetic resonance spin-lattice relaxation of polymer chains confined in tubes: Analytical treatment and Monte Carlo simulation of the crossover from Rouse to reptation dynamics

Alexei Denissov, Margarita Kroutieva, and Nail Fatkullin
Kazan State University, Department of Molecular Physics, 420008 Kazan, Tatarstan, Russia

Rainer Kimmich
Universität Ulm, Sektion Kernresonanzspektroskopie, 89069 Ulm, Germany

(Received 31 October 2001; accepted 27 December 2001)

The frequency and molecular mass dependences of nuclear magnetic resonance spin-lattice relaxation and the time dependence of the mean-squared segment displacement of Kuhn segment chains confined in static straight and randomly coiled tubes with ''soft'' and ''hard'' walls were studied. ''Soft'' walls were modeled in the form of a cylindrical distribution of a harmonic radial potential. This scenario is analytically solvable in contrast to the situation of ''hard'' (reflecting) walls corresponding to an infinitely deep square-well radial potential. In the latter case, we have therefore employed Monte Carlo simulations using a modified Stockmayer chain model. In both situations, qualitatively equivalent results were obtained. Depending on the effective tube diameter (or width of the potential well) a crossover from Rouse to reptation behavior occurs which sets on already far beyond the Flory radius of the polymer. In terms of the spin-lattice relaxation dispersion, reptation reveals itself by $T_1 \propto M^0 \omega^{3/4}$ in the chain mode regime, in good agreement with experimental data for polymers in artificial tubes reported in our previous paper by Kimmich *et al.* [Chem. Phys. Lett. **307**, 147 (1999)]. © *2002 American Institute of Physics.*
[DOI: 10.1063/1.1451242]

I. INTRODUCTION

Triggered by de Gennes' pioneering work[1] of 1971 numerous attempts have been undertaken to describe the dynamics of entangled chains by the assumption of a fictitious tube representing the ''matrix'' surrounding a tagged chain. The more elaborated version of the tube/reptation model in Ref. 2 thus became a standard model in polymer science.

In previous papers[3–5] we reported on nuclear magnetic resonance (NMR) relaxation and diffusion experiments with polymer chains confined in artificial ''tubes'' in a quasi-rigid polymer matrix.[6] One of the most conspicuous findings was that the deuteron spin-lattice relaxation time, T_1, of confined polymer chains obeys a power law for the molecular weight (M) and frequency ($\omega = 2\pi\nu$) dependences,

$$T_1 \propto M^0 \omega^{0.75}, \tag{1}$$

in a wide range. This power law was predicted by de Gennes[1] for longitudinal Rouse modes in a range limited at short times (corresponding to high frequencies) by the chain relaxation time of the mode corresponding to the tube width, the so-called ''entanglement'' time τ_e, and at long times (corresponding to low frequencies) by the longest Rouse relaxation time, τ_R. De Gennes' prediction[1] for chain dynamics ''in the presence of fixed obstacles'' was, thus, experimentally verified in full accordance to the theory even for situations, when the pore radius was rather close to the Flory radius of the macromolecule.

By way of contrast, the ω dependence in bulk melts of the same polymer,[4,5] as well as with many other polymer species,[7,8] was found to be completely different and much weaker. A behavior corresponding to Eq. (1) was never observed although the frequency and the molecular weight were varied in extremely wide ranges. Molecular weights ranging from the critical value, M_c, up to several millions were examined in a proton frequency range 10^3 Hz$< \omega/2\pi <10^8$ Hz, employing the field-cycling NMR relaxometry technique.[9] A frequency dependence approaching that given in Eq. (1) was never found with bulk melts contrary to polymers confined in artificial tubes.

Rouse dynamics is expected for unconfined polymer chains in a viscous medium without backflow effects.[2] In this case the spin-lattice relaxation dispersion is predicted to obey[10–13]

$$T_1 = -\frac{\beta}{\tau_s \ln(\omega\tau_s)} \quad (\omega\tau_s \ll 1), \tag{2}$$

where β is a constant and τ_s is the Rouse relaxation time of a Kuhn segment corresponding to the shortest mode possible. A frequency dependence of this type was indeed observed[8,12–15] in melts of different polymer species with molecular weights $M < M_c$, but by no means above M_c. It is obvious that with Eqs. (1) and (2) the two most prominent theories of polymer dynamics, namely, the tube/reptation model and the Rouse model, can readily be distinguished by way of NMR relaxometry. The spin-lattice relaxation dispersions expected for these models are entirely different and can easily be recognized in experiments.

The purpose of the present work is to study the dynamics of chains of varying length in model tubes of varying diam-

eter and varying chain/wall interaction potentials. As far as possible, an analytical treatment was carried out. This is to be compared with a series of Monte Carlo computer simulations. The objective is to learn how the confinement affects chain dynamics. There is considerable interest in dynamic properties of polymeric liquids confined in tubelike regions, which is stimulated both by practical application aspects and fundamental questions of polymer dynamics. A number of corresponding computer simulations have already been reported in Refs. 16–19.

As an aymptotically analytically solvable problem, we will consider a Rouse chain[2] confined in a harmonic radial potential with cylindrical symmetry, that is, in a stretched, infinitely long tube with ''soft'' walls. The Monte Carlo simulations refer to a generalized Stockmayer chain[20] in an infinitely long cylindrical pore with ''hard'' walls. It will turn out that both models give qualitatively similar results. Then, using an asymptotically exact ansatz, the results will be generalized to the case of tubes having random walk conformation.

II. BASIC THEORY OF THE DYNAMICS OF A KUHN SEGMENT CHAIN IN A STRAIGHT CYLINDRICAL TUBE WITH HARMONIC RADIAL POTENTIAL

A. Definition of the effective tube diameter for a harmonic radial potential

Consider a radial potential acting in the plane x_1,x_2 according to

$$U(\rho)=\frac{\kappa}{2}\rho^2. \tag{3}$$

The constant κ characterizes the potential strength, the variable ρ is the radial distance from the center line of the cylindrical pore given in Cartesian coordinates by $\rho=\sqrt{x_1^2+x_2^2}$. The normalized spatial distribution function (or probability density) of a particle placed in this potential obeys the Boltzmann expression

$$W(x_1,x_2)=\frac{\kappa}{2\pi kT}\exp\left\{-\frac{\kappa}{2kT}\rho^2\right\}, \tag{4}$$

where k is the Boltzmann constant, and T is the absolute temperature. In thermal equilibrium the mean-squared projection of the particle's position vector on the plane x_1,x_2 is equal to

$$\langle\rho^2\rangle=\int\int dx_1dx_2\rho^2W(x_1,x_2)=\frac{2kT}{\kappa}. \tag{5}$$

The effective diameter of the potential given in Eq. (3) may then be defined by

$$\tilde{d}\equiv 2\sqrt{\frac{2kT}{\kappa}}. \tag{6}$$

In terms of $\tilde{d}$ the potential $U(\rho)$ can be rewritten as

$$U(\rho)=\frac{4kT}{\tilde{d}^2}(x_1^2+x_2^2)=\frac{4kT}{\tilde{d}^2}\rho^2. \tag{7}$$

B. Equilibrium distribution and mean-squared values of the normal coordinates of a Kuhn segment chain in a harmonic radial potential

The conformation of a Rouse chain is determined by a set $\{\mathbf{r}_n(t)\}$ of the position vectors of its segments, where the position vector of the nth segment at time t is $\mathbf{r}_n(t)$. The effective intramolecular potential energy of a Rouse chain is given by (see for example Refs. 1, 2, and 21)

$$U_0\{\mathbf{r}_n(t)\}=\sum_{n=1}^{N-1}\frac{3kT}{2b^2}(\mathbf{r}_{n+1}(t)-\mathbf{r}_n(t))^2, \tag{8}$$

where b is the length of a Kuhn segment which may be identified with the Rouse length. In a harmonic radial potential the total energy of a Rouse chain thus reads

$$\begin{aligned}U\{\mathbf{r}_n(t)\}&=U_0\{\mathbf{r}_n(t)\}+\sum_n\frac{4kT}{\tilde{d}^2}\rho_n^2\\&=\sum_n\left\{\frac{3kT}{2b^2}(\mathbf{r}_{n+1}(t)-\mathbf{r}_n(t))^2+\frac{4kT}{\tilde{d}^2}(x_{1n}^2+x_{2n}^2)\right\}.\end{aligned} \tag{9}$$

The Rouse normal coordinates are given by the continuum-limit transformation[1,2,21]

$$\mathbf{X}_p(t)\equiv\frac{1}{N}\int_0^N dn\mathbf{r}_n\cos\left(\frac{\pi}{N}pn\right)\quad(p=0,1,2,\ldots,N-1) \tag{10}$$

and

$$\mathbf{r}_n=\mathbf{X}_0+2\sum_{p=1}^{N-1}\mathbf{X}_p\cos\left(\frac{\pi}{N}pn\right)\quad(n=1,2,3,\ldots,N), \tag{11}$$

where N is the number of Kuhn segments per chain. In terms of normal coordinates $\mathbf{X}_p$, the potential energy $U\{\mathbf{r}_n\}$ can be rewritten as

$$\begin{aligned}U\{\mathbf{r}_n\}&=U\{\mathbf{X}_p\}\\&=\frac{3kT}{2l^2}\sum_{n=1}^{N-1}\left[2\sum_{p=1}^{N-1}\mathbf{X}_p\left(\cos\left(\frac{\pi}{N}p(n+1)\right)-\cos\left(\frac{\pi}{N}pn\right)\right)\right]^2+\sum_{n=1}^{N}\frac{4kT}{\tilde{d}^2}\\&\quad\times\sum_{\alpha=1,2}\left[X_{0\alpha}+2\sum_{p=1}^{N-1}X_{p\alpha}\cos\left(\frac{\pi}{N}pn\right)\right]^2,\end{aligned} \tag{12}$$

where $\mathbf{X}_p=\{X_{p\alpha}\}=(X_{p1},X_{p2},X_{p3})$. Employing the relation

$$\begin{aligned}&\cos\left(\frac{\pi}{N}pn\right)-\cos\left(\frac{\pi}{N}p(n+1)\right)\\&\quad=2\sin\left(\frac{\pi}{N}p\left(n+\frac{1}{2}\right)\right)\sin\left(\frac{\pi}{2N}p\right),\end{aligned} \tag{13}$$

we obtain

$$U\{\mathbf{X}_p\}=\frac{kT}{2}\sum_{\substack{p=1\\ \alpha=1,2}}^{N-1}\left\{\frac{24N}{b^2}\sin^2\left(\frac{\pi}{2N}p\right)+\frac{16N}{\tilde{d}^2}\right\}X_{p\alpha}^2 + \frac{kT}{2}\sum_{p=1}^{N-1}\frac{24N}{b^2}\sin^2\left(\frac{\pi}{2N}p\right)X_{p3}^2 + \frac{4kTN}{\tilde{d}^2}(X_{01}^2+X_{02}^2), \tag{14}$$

where we have used the orthogonality property of normal coordinates. The distribution function of the normal coordinates follows from the Boltzmann distribution as

$$W\{\mathbf{X}_p\}=\frac{1}{Z}\exp\left\{-\frac{1}{kT}U\{\mathbf{X}_p\}\right\}, \tag{15}$$

where

$$Z\equiv\int\prod_{p,\alpha}dX_{p\alpha}W\{\mathbf{X}_p\}$$

is a normalization constant. The potential energy $U\{\mathbf{X}_p\}$ has a diagonal quadratic form with respect to $X_{p\alpha}$. Equation (15) can therefore be represented as a multidimensional Gaussian of the form

$$W\{\mathbf{X}_p\}=\prod_{\substack{p=0\\ \alpha=1,2,3}}^{N-1}\left(\frac{1}{2\pi\langle X_{p\alpha}^2\rangle}\right)^{1/2}\exp\left\{-\frac{1}{2}\frac{X_{p\alpha}^2}{\langle X_{p\alpha}^2\rangle}\right\}, \tag{16}$$

where $\langle X_{p\alpha}^2\rangle$ is the mean-squared value of $X_{p\alpha}^2$. From expressions (14)–(16) the following relations for the equilibrium mean-squared values of the normal modes can be derived:

$$\frac{1}{\langle X_{p\alpha}^2\rangle}=\frac{1}{\langle X_{p\alpha}^2\rangle_0}+\frac{16N}{\tilde{d}^2}\quad(\alpha=1,2), \tag{17}$$

$$\frac{1}{\langle X_{p3}^2\rangle}=\frac{1}{\langle X_{p3}^2\rangle_0}, \tag{18}$$

where

$$\langle X_{p\alpha}^2\rangle_0=\frac{b^2}{24N\sin^2\left(\frac{\pi}{2N}p\right)}\quad(\alpha=1,2,3) \tag{19}$$

is the equilibrium value of the α component of the pth normal coordinate of the free Rouse chain. Note, that for $N\to\infty$, i.e., in the continuum limit, Eq. (19) becomes

$$\langle X_{p\alpha}^2\rangle_0=\frac{Nb^2}{6\pi^2p^2}\quad(\alpha=1,2,3), \tag{20}$$

which is identical to the relation known from the literature.[2,21]

With Eqs. (17) and (18) it becomes obvious that the harmonic radial potential changes the spatial distribution of the polymer segments in the x_1,x_2 plane, where the harmonic force attracts segments towards the symmetry axis (x_3), whereas there is no change in x_3 direction relative to a Gaussian coil.

C. Equations-of-motion and time-dependent correlation functions

The Langevin equation of the nth segment of a Rouse chain in an external potential can be written as

$$m\ddot{\mathbf{r}}_n(t)=-\zeta\dot{\mathbf{r}}_n(t)-\frac{\partial}{\partial\mathbf{r}_n}U\{\mathbf{r}_n\}+\mathbf{f}_{\mathrm{Ln}}(t), \tag{21}$$

where ζ is the local segment friction coefficient, m is the mass of a Kuhn segment,

$$-\frac{\partial}{\partial\mathbf{r}_n}U\{r_n\}$$

is an external force acting on the nth segment, $\mathbf{f}_{\mathrm{Ln}}(t)$ is the stochastic Langevin force the nth segment is subject to. For times $t\gg m/\zeta\simeq10^{-13}$ s, the acceleration term in Eq. (21) can be neglected.[2,21] Inserting Eq. (9) then gives

$$\zeta\frac{\partial}{\partial t}\mathbf{r}_n(t)=\frac{3kT}{b^2}(\mathbf{r}_{n+1}(t)+\mathbf{r}_{n-1}(t)-2\mathbf{r}_n(t)) - \frac{8kT}{d_e^2}\boldsymbol{\rho}_n+\mathbf{f}_{\mathrm{Ln}}(t), \tag{22}$$

where $\boldsymbol{\rho}_n=x_{n1}\mathbf{e}_1+x_{n2}\mathbf{e}_2$, and $\mathbf{e}_1$ and $\mathbf{e}_2$ are unit vectors along the x_1 and x_2 axes, respectively. Multiplying both sides of Eq. (22) with $\cos((\pi/N)pn)$ and integrating over n, leads after some elementary algebra to the following expressions for the normal coordinates $X_{p\alpha}(t)$ [see Eq. (10)]:

$$\begin{aligned}\dot{X}_{p2}(t)&=-\left(\frac{1}{\tau_p}+\frac{1}{\tau_e}\right)\dot{X}_{p2}(t)+\hat{f}_{p2}^L(t),\\ \dot{X}_{p1}(t)&=-\left(\frac{1}{\tau_p}+\frac{1}{\tau_e}\right)\dot{X}_{p1}(t)+\hat{f}_{p1}^L(t),\\ \dot{X}_{p3}(t)&=-\frac{1}{\tau_p}\dot{X}_{p3}(t)+\hat{f}_{p3}^L(t),\end{aligned} \tag{23}$$

where

$$\frac{1}{\tau_p}=\frac{4}{\pi^2}\frac{1}{\tau_s}\sin^2\left(\frac{\pi}{2}\frac{p}{N}\right) \tag{24}$$

is the relaxation rate of the pth normal mode of the free Rouse chain,

$$\frac{1}{\tau_e}=\frac{8}{3\pi^2}\left(\frac{b}{\tilde{d}}\right)^2\frac{1}{\tau_s} \tag{25}$$

is the mode relaxation rate associated with the effective diameter of the harmonic radial potential,

$$\frac{1}{\tau_e}=3\pi^2\frac{kT}{b^2\zeta} \tag{26}$$

is the Rouse segment relaxation rate, and $\hat{f}_{p\alpha}^L$ is the stochastic Langevin force acting on the α component of the pth normal coordinate. The quantity τ_e defined in Eq. (25) corresponds to the so-called ''entanglement time'' defined in the conventional reptation model.[2] For $t\ll\tau_e$ the chain is expected to move like a free Rouse chain, whereas for $t\gg\tau_e$, its motion perpendicular to the tube axis becomes restricted.

Equation (23) can be written in a more compact way

$$\dot{X}_{p\alpha}(t) = -\frac{1}{\tau_{p\alpha}}\dot{X}_{p\alpha}(t) + \hat{f}^L_{p\alpha}(t), \tag{27}$$

where

$$\frac{1}{\tau_{p\alpha}} = \frac{1}{\tau_p} + \frac{1}{\tau_e} \quad \text{for } \alpha = 1,2 \text{ (components transverse to the cylinder axis)} \tag{28}$$

and

$$\frac{1}{\tau_{p3}} = \frac{1}{\tau_p} \quad \text{for } \alpha = 3 \text{ (component along cylinder axis).} \tag{29}$$

The quantity $\tau_{p\alpha}$ is the relaxation time of the α component of the pth normal coordinate. In the continuum limit $N \to \infty$, the mode relaxation rate given in Eq. (24) takes the form known from literature[2]

$$\frac{1}{\tau_p} = \frac{1}{\tau_s}\left(\frac{p}{N}\right)^2. \tag{30}$$

Multiplying both sides of Eq. (27) with $X_{m\beta}(0)$ and averaging over all realizations of $\hat{f}^L_{p\alpha}$ we get

$$\frac{d}{dt}\langle X_{p\alpha}(t)X_{m\beta}(0)\rangle = -\frac{1}{\tau_{p\alpha}}\langle X_{p\alpha}(t)X_{m\beta}(0)\rangle. \tag{31}$$

Note that $\langle \hat{f}^L_{p\alpha}(t)X_{m\beta}(0)\rangle = 0$ due to orthogonality and the absence of any correlation of the stochastic force with the normal coordinates.

The solution of Eq. (31) is

$$\langle X_{p\alpha}(t)X_{m\beta}(0)\rangle = \delta_{\alpha\beta}\delta_{pm}\langle X^2_{p\alpha}\rangle \exp\left\{-\frac{1}{\tau_{p\alpha}}\right\}, \tag{32}$$

where $\langle X^2_{p\alpha}\rangle$ is given by Eqs. (17) and (18). The Kronecker δ-symbols reflect the orthogonality between the normal coordinates on the one hand and between their components on the other. Knowing the distribution of the mode relaxation times $\tau_{p\alpha}$ and the equilibrium mean-squared values of the normal modes $\langle X^2_{p\alpha}\rangle$ permits one to calculate all dynamical characteristics of the Rouse chain moving in a harmonic radial potential.

III. THEORY OF THE CURVILINEAR MEAN-SQUARED DISPLACEMENT OF A KUHN SEGMENT CHAIN IN A TUBE WITH HARMONIC RADIAL POTENTIAL

The mean-squared displacement along the x_α axis, $\alpha = 1,2,3$, can be derived on the basis of the standard normal mode formalism:[2,21]

$$\begin{aligned}\overline{\langle (r_{n\alpha}(t) - r_{n\alpha}(0))^2\rangle} &= \langle (X_{0\alpha}(t) - X_{0\alpha}(0))^2\rangle \\ &\quad + 4\sum_{p=1}^{N-1}\left(1 - \exp\left\{-\frac{t}{\tau_{p\alpha}}\right\}\right)\langle X^2_{p\alpha}\rangle.\end{aligned} \tag{33}$$

The first term on the right-hand side describes center-of-mass displacements along the α-axis. The second term represents displacements relative to the center-of-mass. Note that Eq. (33) refers to an average over all segments of a chain (subscript n) indicated by the bar.

The external harmonic radial potential acts along the x_1 and x_2 axes. Displacements in these directions will therefore be restricted for times $t \gg \tau_e$. The mean-squared displacement in the plane x_1, x_2 is given by

$$\begin{aligned}&\overline{\langle (\boldsymbol{\rho}_n(t) - \boldsymbol{\rho}_n(0))^2\rangle} \\ &= \overline{\langle (x_{n1}(t) - x_{n1}(0))^2\rangle} + \overline{\langle (x_{n2}(t) - x_{n2}(0))^2\rangle} \\ &= 2\langle (X_{01}(t) - X_{01}(0))^2\rangle \\ &\quad + 8\sum_{p=1}^{N-1}\left(1 - \exp\left\{-\frac{t}{\tau_{p1}}\right\}\right)\langle X^2_{p1}(0)\rangle.\end{aligned} \tag{34}$$

In the limit $t \gg \tau_e$, Eq. (33) can be rewritten as

$$\begin{aligned}\langle (\delta\rho)^2\rangle &\equiv \overline{\langle (\boldsymbol{\rho}_n(\infty) - \boldsymbol{\rho}_n(0))^2\rangle} \\ &= 2\langle X^2_{01}(\infty)\rangle - 4\langle X_{01}(\infty)X_{01}(0)\rangle \\ &\quad + 2\langle X^2_{01}(0)\rangle + 8\sum_{p=1}^{N-1}\langle X^2_{p1}(0)\rangle \\ &= 4\langle X^2_{01}(0)\rangle + 8\sum_{p=1}^{N-1}\langle X^2_{p1}(0)\rangle.\end{aligned} \tag{35}$$

Using Eqs. (17) and (18) we can represent formula (35) as

$$\langle (\delta\rho)^2\rangle = \frac{\tilde{d}^2}{4N} + 8\sum_{p=1}^{N-1}\frac{\langle X^2_{p1}(0)\rangle_0 \dfrac{\tilde{d}^2}{16N}}{\langle X^2_{p1}(0)\rangle_0 + \dfrac{\tilde{d}^2}{16N}}. \tag{36}$$

The quantity $\langle X^2_{p\alpha}(0)\rangle_0$ given in Eq. (19) is valid for free Rouse normal modes. On this basis, Eq. (36) can be evaluated numerically. However, in the continuum limit $N \to \infty$, it can also be calculated asymptotically exactly by using Eq. (20) and replacing the sum by an integral over p:

$$\begin{aligned}\langle (\delta\rho)^2\rangle &= \frac{\tilde{d}^2}{4N} + 8\int_1^{N-1} dp \frac{\dfrac{Nb^2}{6\pi^2p^2}\dfrac{\tilde{d}^2}{16N}}{\dfrac{Nb^2}{6\pi^2p^2} + \dfrac{\tilde{d}^2}{16N}} \\ &= \frac{\tilde{d}^2}{4N} + \sqrt{\frac{2}{3}}\frac{\tilde{d}b}{\pi}\left[\arctan\left(\sqrt{\frac{3}{8}}\pi\frac{\tilde{d}}{b}\right)\right. \\ &\quad \left. - \arctan\left(\sqrt{\frac{3}{8}}\pi\frac{\tilde{d}}{Nb}\right)\right] \\ &\simeq \sqrt{\frac{2}{3}}\frac{\tilde{d}b}{\pi}\arctan\left(\sqrt{\frac{3}{8}}\pi\frac{\tilde{d}}{b}\right).\end{aligned} \tag{37}$$

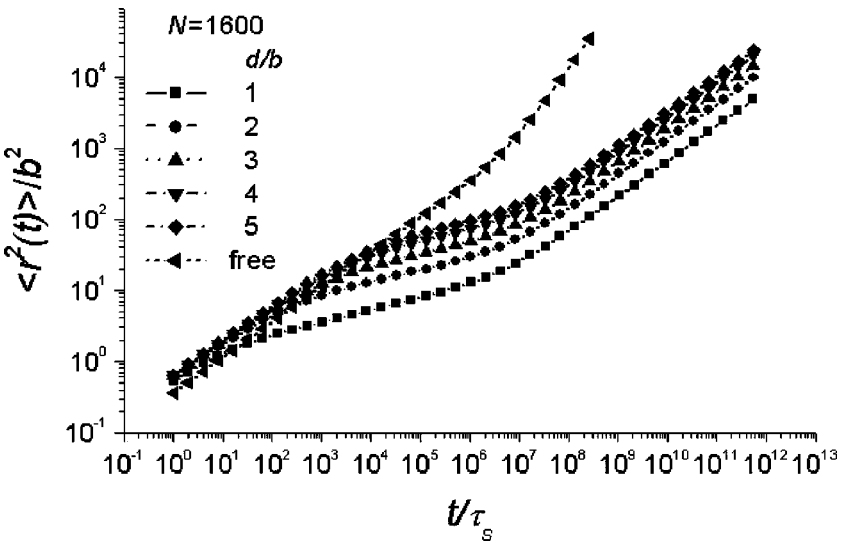

FIG. 1. Mean-squared segment displacement for a chain with $N=1600$ Kuhn segments confined in a randomly coiled tube of different effective tube diameters d. The data have been evaluated from Eq. (42) modified for Gaussian tube conformations and refer to displacements in the laboratory frame. In the short-time regime $\tau_s \ll t \ll \tau_e$, the curves exhibit the $t^{1/2}$ dependence expected for free Rouse chains. At medium times the $t^{1/4}$ power law characteristic for reptation in the limit $\tau_e \ll t \ll \tau_R$ follows. At times longer than τ_R finally a $t^{1/2}$ power law shows up which represents coherent chain diffusion along the tube. The intermediate regime is shifted to shorter times with more narrow effective tube diameters d because of the increasing influence of the topological constraints by the tube. Note that free Rouse chains are characterized by a proportionality to $t^{1/2}$. This proportionality is approached in the limit of large effective tube diameters.

If the effective diameter $\tilde{d}$ of the harmonic radial potential is much larger than the Kuhn segment length b, i.e.,

$$\sqrt{\frac{3}{8}}\pi\frac{\tilde{d}}{b} \gg 1,$$

Eq. (37) takes the simple form

$$d^2 \equiv \langle(\delta\rho)^2\rangle \simeq \frac{1}{\sqrt{6}}\tilde{d}b. \tag{38}$$

In the sense of the tube/reptation model[2] the characteristic length d defined by Eq. (38) can be considered as an effective tube diameter for chains long enough, i.e., $N\to\infty$, placed in a radial harmonic potential. From Eq. (38) it follows that

$$d \simeq \left(\frac{1}{6}\right)^{1/4}\sqrt{\tilde{d}b} \ll \tilde{d}. \tag{39}$$

The effective tube diameter d for a harmonic radial potential for long macromolecules is much smaller than the effective harmonic potential diameter $\tilde{d}$ for short chains. This reduction of the effective tube diameter is a direct consequence of the chain connectivity that leads to a strong sensitivity to external space restrictions.

For $t \ll \tau_e$, Eq. (34) predicts anomalous diffusion in any direction as expected for free Rouse dynamics,

$$\langle(\delta\rho(t))^2\rangle \simeq \frac{4}{3\pi^{3/2}}b^2\left(\frac{t}{\tau_s}\right)^{1/2}. \tag{40}$$

In the opposite limit, $t \gg \tau_e$, displacements perpendicular to the tube axis are restricted to the effective tube diameter d. Both limits for transverse displacements can be combined using Eqs. (38) and (40) to a simple analytical expression which gives the correct asymptote in the continuum limit. The final result for the mean-squared transverse displacements thus is

$$\langle(\delta\rho(t))^2\rangle \simeq \frac{4}{3\pi^{3/2}}b^2\left(\frac{t}{\tau_s}\right)^{1/2}\frac{1}{1+\dfrac{4}{3\pi^{3/2}}\dfrac{b^2}{d^2}\left(\dfrac{t}{\tau_s}\right)^{1/2}}. \tag{41}$$

On the other hand, longitudinal displacements along the x_3 axis are not influenced by the harmonic potential, and the corresponding mean-squared longitudinal displacement consequently corresponds to that expected for a free Rouse chain:

$$\begin{aligned}\langle\delta x_3^2(t)\rangle &\equiv \overline{\langle(r_{n3}(t)-r_{n3}(0))^2\rangle} \\ &\simeq \frac{2}{3\pi^2}\frac{b^2}{N}\frac{t}{\tau_s} + \frac{2}{3\pi^{3/2}}b^2\left(\frac{t}{\tau_s}\right)^{1/2} \\ &\quad\times\frac{1}{1+\dfrac{6}{\pi^{3/2}N}\left(\dfrac{t}{\tau_s}\right)^{1/2}}.\end{aligned} \tag{42}$$

Note that this expression is again a simple analytical approximation of the exact formula [Eq. (33)] for $\alpha=3$ in the continuum limit that gives correct asymptotic expressions for the limits $\tau_s \ll t \ll \tau_R$ and $t \gg \tau_R$, where $\tau_R = \tau_s N^2$ is the Rouse relaxation time.

Equation (42) refers to curvilinear segment displacements along the axis of a tube with harmonic radial potential. If the tube has a Gaussian conformation, the laboratory frame mean-squared segment displacement has a reduced time dependence. Figure 1 represents a corresponding evaluation of Eq. (42) modified for a random coil geometry. The three anomalous diffusion regimes predicted by Doi and Edwards for the ordinary tube model also show up for the present case where the chain is considered to be confined in a tubelike region with a harmonic radial potential. The dependence on the effective tube diameter indicates how the different degrees of topological constraints affect the mean-squared segment displacement. In this respect, it is thus demonstrated that the ''soft'' tube considered here is equivalent to the ordinary Doi/Edwards tube. Using polymers confined in artifi-

cial tubes formed by pores in a solid matrix, some of the characteristic features of the anomalous diffusion regime were recently demonstrated in fringe-field NMR diffusometry experiments[3,5] in good agreements with the theoretical predictions.

IV. CORRELATION FUNCTION OF THE TANGENT VECTOR FOR A KUHN SEGMENT CHAIN IN A STRAIGHT TUBE WITH HARMONIC RADIAL POTENTIAL

The tangent vector of Kuhn segments is determined by the relation

$$\mathbf{b}_n(t) \equiv \mathbf{r}_{n+1}(t) - \mathbf{r}_n(t). \tag{43}$$

Expressed in normal coordinates according to Eq. (11) it reads

$$\begin{aligned}\mathbf{b}_n(t) &= 2\sum_{p=1}^{N-1} \mathbf{X}_p(t)\left[\cos\left(\frac{\pi}{N}p(n+1)\right) - \cos\left(\frac{\pi}{N}pn\right)\right] \\ &= -4\sum_{p=1}^{N-1} \mathbf{X}_p(t)\sin\left(\frac{\pi}{N}p\left(n+\frac{1}{2}\right)\right)\sin\left(\frac{\pi}{2N}p\right).\end{aligned} \tag{44}$$

The autocorrelation function of components of the tangent vector thus becomes

$$\langle b_\alpha(t)b_\beta(0)\rangle = 8\,\delta_{\alpha\beta}\sum_{p=1}^{N-1}\langle X_{p\alpha}(t)X_{p\alpha}(0)\rangle \sin^2\left(\frac{\pi}{2N}p\right), \tag{45}$$

where we anticipate an average over all Kuhn segments n of a chain. In the continuum limit we have

$$\langle b_\alpha(t)b_\alpha(0)\rangle = \frac{2\pi^2}{N^2}\sum_{p=1}^{N-1} p^2\langle X_{p\alpha}(t)X_{p\alpha}(0)\rangle. \tag{46}$$

These correlation functions of the tangent vector components can be evaluated numerically. On the other hand, there is again the possibility to derive asymptotic expressions in the continuum limit.

Let us start with the initial values for the transverse components

$$\begin{aligned}\langle b_1^2(0)\rangle &= \langle b_2^2(0)\rangle \\ &= \frac{2\pi^2}{N^2}\sum_{p=1}^{N-1} p^2\langle X_{p1}^2(0)\rangle \\ &\cong \frac{2\pi^2}{N^2}\int_1^N \frac{\tilde{d}^2}{16N}\frac{p^2dp}{1+\frac{3\pi^2}{8}\left(\frac{\tilde{d}}{b}\right)^2\left(\frac{p}{N}\right)^2} \\ &= \frac{b^2}{3} - \sqrt{\frac{8}{3}}\frac{1}{3\pi}\frac{b^3}{\tilde{d}}\arctan\left(\sqrt{\frac{3}{8}}\pi\frac{\tilde{d}}{b}\right).\end{aligned} \tag{47}$$

For $N \gg \tilde{d}/b \gg 1$, this expression takes the simple form

$$\langle b_1^2(0)\rangle = \langle b_2^2(0)\rangle \cong \frac{b^2}{3}\left\{1 - \frac{1}{3}\frac{b^2}{d^2}\right\}. \tag{48}$$

For the (unconfined) longitudinal tangent vector component we have

$$\langle b_3^2(0)\rangle = \frac{b^2}{3} \tag{49}$$

as expected for a free Rouse chain. The different forms of Eqs. (48) and (49) reflect the different influence of the harmonic radial potential on the equilibrium distribution of segments in transverse and longitudinal direction.

After a similar calculation we find for the transverse components in the limit $\tau_s \ll t \ll \tau_e$

$$\begin{aligned}\langle b_1(t)b_1(0)\rangle &= \langle b_2(t)b_2(0)\rangle \\ &= \frac{\sqrt{\pi}}{6}b^2\left(\frac{\tau_s}{t}\right)^{1/2}\exp\left\{-\frac{t}{\tau_e}\right\}\end{aligned} \tag{50}$$

and for $\tau_e \ll t \ll \tau_R$

$$\begin{aligned}\langle b_1(t)b_1(0)\rangle &= \langle b_2(t)b_2(0)\rangle \\ &= \frac{\pi^{5/2}}{32}\tilde{d}^2\left(\frac{\tau_s}{t}\right)^{3/2}\exp\left\{-\frac{t}{\tau_e}\right\}.\end{aligned} \tag{51}$$

A simple analytical expression that has both expressions (46) and (47) as asymptotes is given by

$$\begin{aligned}\langle b_1(t)b_1(0)\rangle &= \langle b_2(t)b_2(0)\rangle \\ &= \frac{\sqrt{\pi}}{6}b^2\left(\frac{\tau_s}{t}\right)^{1/2}\frac{1}{1+2\frac{t}{\tau_e}}\exp\left\{-\frac{t}{\tau_e}\right\},\end{aligned} \tag{52}$$

where we have made use of Eq. (25). The result for the (unconfined) longitudinal component again corresponds to the ordinary Rouse theory in the limit $\tau_s \ll t \ll \tau_R$

$$\langle b_3(t)b_3(0)\rangle = \frac{\sqrt{\pi}}{6}b^2\left(\frac{\tau_s}{t}\right)^{1/2}. \tag{53}$$

V. SPIN-LATTICE RELAXATION OF A KUHN SEGMENT CHAIN IN A STRAIGHT TUBE WITH HARMONIC RADIAL POTENTIAL

Proton spin-lattice relaxation in polymer melts is determined by magnetic dipole-dipole interactions.[9,22] In the case of deuterons the dominating spin interaction is electric quadrupole coupling to molecular electric-field gradients. Spin-lattice relaxation is a consequence of molecular fluctuations, which commonly modulate both types of spin interactions. Consequently, the theories of spin-lattice relaxation of protons and deuterons are equivalent, apart from factors characterizing the type and the strength of the couplings and parameters specific for the spin-bearing nuclei. In the following we will first elaborate the theory for dipolar coupled spins I and then turn to quadrupole nuclei with spin $I=1$.

A. Dipole-dipole coupling

In this case, the spin-lattice relaxation rate can generally be expressed by

$$\frac{1}{T_1}=3\gamma^2\hbar^2 I(I+1)\int_0^\infty dt\{\cos(\omega t)L^{z+}(t)+\cos(2\omega t)L^{++}(t)\},\tag{54}$$

where γ is the gyromagnetic ratio, $\hbar$ is the Planck constant divided by 2π, $L^{z+}(t)$ and $L^{++}(t)$ are dipole–dipole correlation functions defined by

$$L^{z+}(t)\equiv\frac{1}{N_s}\sum_{i\neq j}\left\langle\frac{e_{ij}^z(t)e_{ij}^+(t)e_{ij}^z(0)e_{ij}^-(0)}{r_{ij}^3(t)r_{ij}^3(0)}\right\rangle_{eq},\tag{55}$$

$$L^{++}(t)\equiv\frac{1}{N_s}\sum_{i\neq j}\left\langle\frac{(e_{ij}^+(t))^2(e_{ij}^-(0))^2}{r_{ij}^3(t)r_{ij}^3(0)}\right\rangle_{eq}.\tag{56}$$

where N_s is the total number of spins in a sample, $\mathbf{e}_{ij}(t)\equiv\mathbf{r}_{ij}(t)/r_{ij}(t)$ is the unit vector directed from spin i to spin j, $r_{ij}(t)$ is the interspin distance at time t, $e_{ij}^+(t)\equiv e_{ij}^x(t)+ie_{ij}^y(t)$, $e_{ij}^-(t)\equiv e_{ij}^x(t)-ie_{ij}^y(t)$, $e_{ij}^\alpha(t)$ is the α component of $\mathbf{e}_{ij}(t)$ with $\alpha=x,y,z$ representing the laboratory frame coordinates. The averages in Eqs. (55) and (56) refer to fluctuations in thermal equilibrium (brackets) as well as to all possible spin pairs in the system (sums). The functions given in Eqs. (55) and (56) strongly depend on the interspin distance. The consequence is that the initial values $L^{z+}(0)$ and $L^{++}(0)$ are determined by spins belonging to the same Kuhn segment. This means, that at least for frequencies high enough the spin-lattice relaxation rate is also determined by the interactions of spins belonging to the same Kuhn segment. We will therefore restrict ourselves to contributions from intrasegment spin interactions. For an extended discussion of intra-versus intersegment interactions and experimental data, see Refs. 7 and 23.

Consider now two spins labeled i and j and belonging to the segment number n of the reference polymer. Equation (56), for example, is based on the vector $\mathbf{e}_{ij}(t)/r_{ij}^{3/2}(t)$, which can be represented as a sum of two orthogonal vectors

$$\frac{\mathbf{e}_{ij}(t)}{r_{ij}^{3/2}(t)}=\frac{\mathbf{b}_n(t)}{b_n(t)}\left\langle\frac{\mathbf{b}_n(t)}{b_n(t)}\cdot\frac{\mathbf{e}_{ij}(t)}{r_{ij}^{3/2}(t)}\right\rangle+\left\{\frac{\mathbf{e}_{ij}(t)}{r_{ij}^{3/2}(t)}-\frac{\mathbf{b}_n(t)}{b_n(t)}\left\langle\frac{\mathbf{b}_n(t)}{b_n(t)}\cdot\frac{\mathbf{e}_{ij}(t)}{r_{ij}^{3/2}(t)}\right\rangle\right\}.\tag{57}$$

The first term on the right-hand side is parallel to the tangent vector $\mathbf{b}_n(t)$, whereas the second term is perpendicular to it. The perpendicular component of $\mathbf{e}_{ij}(t)/r_{ij}^{3/2}(t)$ is subject to much faster fluctuations than the parallel component due to all sorts of local reorientations in the Kuhn segments. That is, correlations based on the perpendicular component will practically have decayed to zero on a time scale $t\gg\tau_s$. This is in contrast to the parallel component which specifically probes chain modes on a much longer time scale. Therefore, it is sufficient to restrict the consideration to the contribution of the parallel component to spin-lattice relaxation, and we may write in good approximation

$$\frac{\mathbf{e}_{ij}(t)}{r_{ij}^{3/2}(t)}\cong\frac{\mathbf{b}_n(t)}{b_n(t)}\left\langle\frac{\mathbf{b}_n(t)}{b_n(t)}\cdot\frac{\mathbf{e}_{ij}(t)}{r_{ij}^{3/2}(t)}\right\rangle.\tag{58}$$

The time dependence of the expression in parentheses is weak, because $\mathbf{b}_n(t)$ and $\mathbf{e}_{ij}(t)$ tend to span a fixed angle for times well above the local segment relaxation time, i.e., for $t\gg\tau_s$. On this time scale the distance between the spin pair i,j also shows little fluctuation so that we may approximate this expression by its thermal equilibrium average,

$$\left\langle\frac{\mathbf{b}_n(t)}{b_n(t)}\cdot\frac{\mathbf{e}_{ij}(t)}{r_{ij}^{3/2}(t)}\right\rangle\cong\left\langle\left\langle\frac{\mathbf{b}_n(t)}{b_n(t)}\cdot\frac{\mathbf{e}_{ij}(t)}{r_{ij}^{3/2}(t)}\right\rangle\right\rangle_{eq}.\tag{59}$$

This sort of argument leads to a new formula for the spin-lattice relaxation rate, Eq. (54), given by

$$\frac{1}{T_1}\simeq\frac{\tilde{M}_2}{b^4}\int_0^\infty dt\{\cos(\omega t)\langle b_n^z(t)b_n^z(0)b_n^+(t)b_n^-(0)\rangle+\cos(2\omega t)\langle(b_n^+(t))^2(b_n^-(0))^2\rangle\},\tag{60}$$

where

$$\tilde{M}_2\equiv\frac{3\gamma^2\hbar^2 I(I+1)}{\tilde{N}_s}\sum_{i\neq j}\left\langle\frac{\mathbf{b}_n(t)}{b}\frac{\mathbf{e}_{ij}(t)}{r_{ij}^{3/2}(t)}\right\rangle_{eq}^4\tag{61}$$

characterizes the strength of the intrasegmental dipole–dipole interaction, $\tilde{N}_s$ is the number of spins in a Kuhn segment. The correlation functions in the braces on the right-hand side of Eq. (60) can be replaced by expressions derived in the appendix. For harmonic potentials, we have, according to Eqs. (83) and (84),

$$\begin{aligned}\langle b^z(t)b^z(0)b^+(t)b^-(0)\rangle&=\tfrac{14}{15}\langle b_1(t)b_1(0)\rangle^2+\tfrac{4}{5}\langle b_1(t)b_1(0)\rangle\langle b_3(t)b_3(0)\rangle\\&\quad+\tfrac{4}{15}\langle b_3(t)b_3(0)\rangle^2+\tfrac{2}{15}\{\langle b_1^2(0)\rangle^2-\langle b_3^2(0)\rangle^2\}^2\end{aligned}\tag{62}$$

and

$$\begin{aligned}\langle(b_n^+(t))^2(b_n^-(0))^2\rangle&=\tfrac{56}{15}\langle b_1(t)b_1(0)\rangle^2+\tfrac{16}{5}\langle b_1(t)b_1(0)\rangle\langle b_3(t)b_3(0)\rangle\\&\quad+\tfrac{16}{15}\langle b_3(t)b_3(0)\rangle^2+\tfrac{8}{15}\{\langle b_1^2(0)\rangle^2-\langle b_3^2(0)\rangle^2\}^2.\end{aligned}\tag{63}$$

The time dependences of the correlation functions of the tangent vector components are given in Eqs. (48)–(53) for different limits.

B. Quadrupole coupling of spins $I=1$

Spin-lattice relaxation of spins $I=1$ tends to be dominated by quadrupole coupling to intramolecular electric-field gradients. An example are deuterons in deuterated diamagnetic systems. The spin-lattice relaxation rate is again given by an expression of the same analytical form[9] as Eq. (60). The only difference is the different physical meaning of the constant $\tilde{M}_2$. The electric-field gradient tensor is fixed in the molecular frame. It is hence linked to the Kuhn segment orientation which is again characterized by the tangent vector $\mathbf{b}_n$.

The quadrupole interaction Hamiltonian in Dirac's representation is[22]

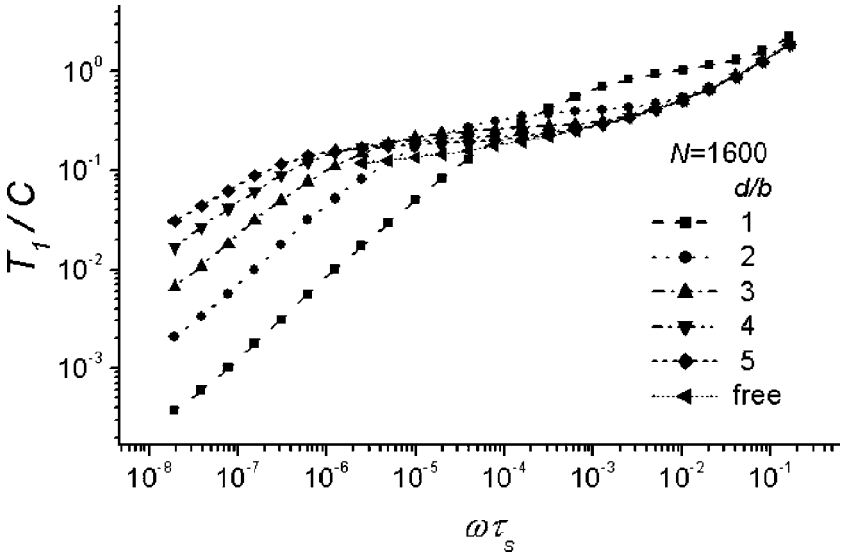

FIG. 2. Spin-lattice relaxation dispersion for a chain of $N=1600$ Kuhn segments confined in randomly coiled tubes with a harmonic radial potential with varying effective diameters d. The constant C is equal to $(\tilde{M}_2\tau_s)^{-1}$. The data have been evaluated based on Eqs. (60)–(63) and Eqs. (69) and (70). At low frequencies the curves visualize the crossover from Rouse dynamics [see Eq. (2)] to reptation [see Eq. (1)] depending on the effective tube diameter. The latter case is characterized by a T_1 dispersion proportional to $\omega^{3/4}$.

$$\hat{\tilde{H}}_Q(t)=\sum_{i,j}\frac{\partial^2 V}{\partial X_i\partial X_j}\hat{\tilde{Q}}_{ij}, \tag{64}$$

where $\partial^2 V/\partial X_i\partial X_j$ is the i,j element of the local electric-field gradient tensor, V is the electrostatic potential, and

$$\hat{\tilde{Q}}_{ij}(t)=\frac{eQ}{6I(2I-1)}\left\{\frac{3}{2}(\hat{\tilde{I}}_i(t)\hat{\tilde{I}}_j(t)+\hat{\tilde{I}}_j(t)\hat{\tilde{I}}_i(t))-\delta_{ij}I(I+1)\right\} \tag{65}$$

is the i,j element of the electric quadrupole moment tensor. The subscripts i and j denote axes of an arbitrarily chosen orthogonal coordinate system. The quantities e and Q are the elementary charge and the nuclear quadrupole moment as such, respectively.

The axis of number $i=1$ may be chosen parallel to $\mathbf{b}_n(t)$, the tangent vector of the nth Kuhn segment. In the limit $t\gg\tau_s$, the only relevant term in the sum in Eq. (64) is that containing the diagonal element of the field gradient tensor $\partial^2 V/\partial^2 X_1$. All other terms are negligible due to averaging by fast fluctuations on this time scale (i.e., for $\omega\tau_s\ll 1$). The quadrupole interaction Hamiltonian can therefore be simplified as

$$\hat{\tilde{H}}_Q(t)\cong\left\langle\frac{\partial^2 V}{\partial^2 X_1}\right\rangle_{\boldsymbol{b}}\frac{eQ}{6I(2I-1)}\left\{3\frac{[\hat{\tilde{\mathbf{I}}}(t)\cdot\mathbf{b}(t)]^2}{b^2}\right\}. \tag{66}$$

The usual perturbation theoretical treatment leads then to

$$\tilde{M}_2\cong\frac{2}{3}\frac{1}{\hbar^2}\left\langle\frac{\partial^2 V}{\partial^2 X_1}\right\rangle_{\boldsymbol{b}}^2 e^2Q^2 \tag{67}$$

instead of Eq. (61). With this quantity, Eq. (60) is valid again. As above, the different time limits given in Eqs. (48)–(53) for the correlation functions of the tangent vector components determine the frequency dependence of the spin-lattice relaxation dispersion in these cases.

VI. SPIN-LATTICE RELAXATION OF A KUHN SEGMENT CHAIN IN A RANDOMLY COILED TUBE

Up to now we have considered polymer chains confined in straight tubes. The consequence is that a finite residual correlation remains in the long-time limit characterizing the topological constraint by the tube. In randomly coiled tubes, this residual correlation decays further down to zero due to curvilinear segment diffusion along the coiled tube axis. There is no exact solution in this case. However, the problem can be discussed asymptotically exactly in the limit $\tilde{l}\gg d$, where $\tilde{l}$ is the persistence length of the randomly coiled tube.

According to Eq. (40), the time needed for curvilinear displacements of order $\tilde{l}$ along the tube axis is about

$$\tilde{t}\simeq\frac{9\pi^3}{16}\left(\frac{\tilde{l}}{b}\right)^4\tau_s. \tag{68}$$

If $\tilde{l}\gg d$, then $\tilde{t}\gg\tau_e=9\pi^2/4(d/b)^4\tau_s$. In the short-time limit, $t\ll\tau_e$, Eqs. (62) and (63) are still valid. At long times, $t\gg\tilde{t}$, the correlation functions are proportional to the probability that a polymer segment is still or again in a range $\tilde{l}$ around the initial position in the tube,

$$P(\tilde{l};t)=\frac{1}{\sqrt{2\pi\langle\delta x_3^2(t)\rangle}}\int_{-\tilde{l}}^{\tilde{l}}\exp\left\{-\frac{x_3^2}{2\langle\delta x_3^2(t)\rangle}\right\}dx_3$$
$$=\mathrm{erf}\left(\frac{\tilde{l}}{\sqrt{2\langle\delta x_3^2(t)\rangle}}\right), \tag{69}$$

and we may employ the approximation

$$\langle A(t)B(0)\rangle_{\mathrm{rep}}\cong\langle A(t)B(0)\rangle P(\tilde{l};t), \tag{70}$$

where $A(t)$ and $B(t)$ represent either $L^{z+}(t)$ or $L^{++}(t)$. The brackets, $\langle\ldots\rangle_{\mathrm{rep}}$, indicate the average over all segment trajectories due to reptation in a randomly coiled tube.

Figure 2 shows a corresponding evaluation of the spin-lattice relaxation dispersion based on Eqs. (60)–(63) and Eqs. (69) and (70). At high frequencies there is little devia-

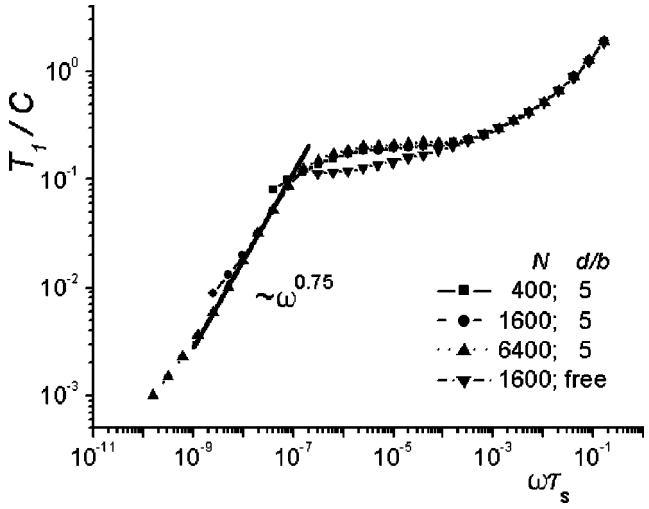

FIG. 3. Spin-lattice relaxation dispersion for chains of different lengths confined in randomly coiled tubes with a harmonic radial potential. The constant C is equal to $(\tilde{M}_2\tau_s)^{-1}$. The data have been evaluated based on Eqs. (60)–(63) and Eqs. (69) and (70). At low frequencies the curves are dominated by reptation, i.e., $T_1 \propto N^0\omega^{3/4}$ [see Eq. (1)]. There is practically no dependence on the chain length. The solid line represents the power law.

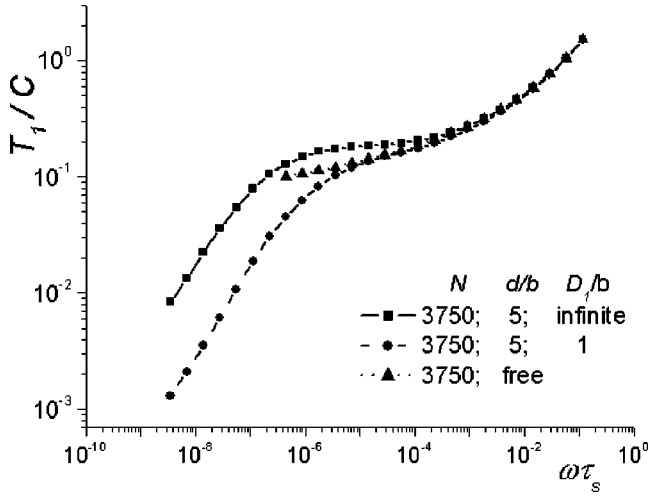

FIG. 4. Spin-lattice relaxation dispersion for a chain confined in randomly coiled tubes with a harmonic radial potential with $(D_1=1)$ and without $(D_1=\infty)$ excluded-volume interaction [see Eq. (72)]. The constant C is equal to $(\tilde{M}_2\tau_s)^{-1}$. The data have been evaluated based on Eqs. (60)–(63) and Eqs. (69) and (70) taking into account Sec. VII. At low frequencies the curves are dominated by reptation, i.e., $T_1 \propto \omega^{3/4}$ [see Eq. (1)], irrespective of the excluded-volume interaction.

tion of the frequency dependence of T_1 expected for free Rouse chains, and the variation with the effective tube diameter is minor. However, in the low-frequency regime the T_1 dispersion adopts the asymptotic $\omega^{3/4}$ law characteristic for reptation in the range $\tau_e^{-1} \ll \omega \ll \tau_R^{-1}$. This is the regime where segments are already probing the tube orientation while being displaced along the randomly coiled tube axis. It is thus shown that de Gennes' original prediction for the ordinary tube model,[1] Eq. (1), is also valid for chains confined in tubes with harmonic radial potentials.

The variation of the effective tube diameter d in Fig. 2 nicely indicates the crossover from Rouse behavior [Eq. (2)] to reptation [Eq. (1)]. The more narrow the tube is, i.e., the stronger the topological constraint effect is, the more pronounced the asymptotic $T_1 \propto \omega^{3/4}$ law shows up.

Figure 3 shows the frequency dependence of T_1 for varying chain lengths at fixed effective tube diameter. The vanishing chain length dependence is obvious as predicted by Eq. (2). The combined $T_1 \propto N^0\omega^{3/4}$ power law predicted for the spin-lattice relaxation dispersion was verified in recent deuteron field cycling NMR relaxometry experiments where deuterated polymers were confined in artificial tubes formed by pores in a solid matrix.[4,5]

VII. EFFECTS DUE TO EXCLUDED-VOLUME INTERACTIONS

A further point to be discussed is the effect of excluded-volume intrachain interactions on chain dynamics. The chain end-to-end distance along the x_3 direction scales as $\sqrt{\frac{1}{3}}b\sqrt{N}$ for a chain with N-Kuhn segments. The chain segment density inside the tube obeys the proportionality

$$\rho_m \propto \frac{N}{d^2 b\sqrt{N}} = \frac{\sqrt{N}}{d^2 b}. \tag{71}$$

Obviously it becomes infinite for $N \to \infty$. That is, the excluded-volume interaction should be taken into account for large N. A simple way to do this, is to introduce a suitable intrachain potential tending to repel the chain ends,

$$U_{eq}(\{x_{3n}\}) = \frac{kT}{D_1}(x_{3N} - x_{30}), \tag{72}$$

where D_1 is a parameter inversely proportional to the strength of the excluded-volume interaction. The average distance between the chain ends along the direction of x_3 then becomes

$$\langle (x_{3N} - x_{30}) \rangle = \frac{b^2 N}{3D_1}, \tag{73}$$

and the projection of the tangent vector b_{3n} takes the average value

$$\langle b_{3n} \rangle = \frac{b^2}{3D_1}. \tag{74}$$

The quantity $b_{3n}(t)$ can be represented as

$$b_{3n}(t) = \langle b_{3n} \rangle + \delta b_{3n}(t), \tag{75}$$

where $\delta b_{3n}(t)$ is the fluctuating part of the x_3 component of the tangent vector.

The above results for the mean-squared displacement and for the tangent vector components $b_{1n}(t)$ and $b_{2n}(t)$ are not affected by the excluded-volume potential given in Eq. (72). This also applies to Eqs. (62) and (63). On the other hand, Eq. (53) for $b_3(t)$ can be corrected by replacing $b_3(t)$ by $\delta b_3(t)$.

Figure 4 shows the numerical evaluation of the above formalism for spin-lattice relaxation of a chain with and without excluded-volume interaction in a randomly coiled tube with harmonic radial potential. Apart from different absolute values of the spin-lattice relaxation time T_1 at low

frequencies, there is little effect of this interaction. At high frequencies, where the reptation mechanism does not yet matter, the effect even vanishes completely.

VIII. COMPUTER SIMULATIONS

Radial potentials other than of a harmonic shape cannot be treated analytically. In the following, Monte Carlo simulations for square-well radial potentials will be described. In addition, the results of the above analytical theory for harmonic radial potentials will be tested in the same way.

As random number generators, two different algorithms, the shuffled linear congruential generator (Lewis, Schrage, Bays, and Durham) and the lagged Fibonacci generator (Mitchel and Moore), were used which are described in the book by Newman and Barkema[24] No dependence on the choice of random number generator was found.

The polymer was modeled in the form of a Stockmayer chain[2,20] modified for our purposes and without excluded-volume interactions. Mean-squared segment displacements were directly determined from the coordinates of the segments as a function of time. The spin-lattice relaxation dispersion was obtained by simulating the correlation functions of the tangent vector components [see Eqs. (62) and (63)] and by then evaluating a numerical Fourier cosine transform according to Eq. (60).

A. The modified Stockmayer chain model

The original Stockmayer model[2,20] assumes a freely jointed segment chain of fixed segment length with some restrictions imposed on the rotational jumps permitted. Only 180° rotational segment jumps around the segment-segment bonds are allowed. Mean-squared displacements of a free chain simulated on this basis are in reasonable agreement with theoretical predictions. However, it turned out that correlation functions of the tangent vector components cannot be simulated reliably with the aid of this simple model. For example, simulations based on the original Stockmayer chain fail to reproduce the theoretically expected proportionality $\langle b_3(t)b_3(0)b_2(t)b_2(0)\rangle \propto \langle b_3(t)b_3(0)\rangle^2$ for a free chain in the long-time limit, as it should be for the Rouse chain.[10,11,25]

We therefore modified this model in the sense that segments are allowed to perform rotational jumps around the segment-segment bonds by angles up to $\pi/2$ only. In our simulation algorithm, a chain segment is chosen at random. Then a random rotation angle within $-\pi/2 \leqslant \varphi \leqslant \pi/2$ is determined with which the segment is rotated. This procedure is repeated step by step.

The simulations were initialized in the following way: First, a point inside the tube was chosen at random. Then the direction of the first segment was randomly determined. The second segment is jointed to the end point of the first segment again with a random direction, and so on. If this random sequence of segment orientations happened to lead to a segment end point outside the tube, the last segment determined in this way was ignored and the procedure was repeated for this segment. In this manner it was made sure that all possible initial conformations occurred with equal probability.

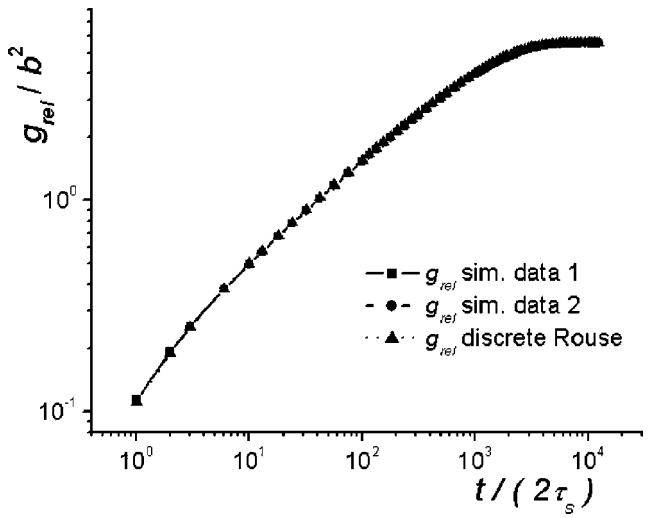

FIG. 5. Test of the modified Stockmayer chain model with a Monte Carlo simulation of the mean-squared segment displacement relative to the center-of-mass of an unconfined chain with $N=50$ Kuhn segments of fixed length without excluded-volume interactions. For comparison, theoretical data for the discrete Rouse model were numerically evaluated according to $g_{\mathrm{rel}} = 4\Sigma_{p=1}^{N-1}\langle X_{\alpha p}(t)X_{\alpha p}(0)\rangle$ [see Eq. (33)]. The time unit in this evaluation was set to $2\tau_s$. In the Monte Carlo simulation, N random rotations per chain and time unit were allowed for. Data sets of two independent simulations are plotted.

B. Test of the modified Stockmayer model with free chains

The Monte Carlo procedure based on the generalized Stockmayer chain model was tested with an unconfined chain. Quantitatively good agreement with analytical predictions for the discrete Rouse chain were obtained as demonstrated in Figs. 5 and 6 for the mean-squared displacement

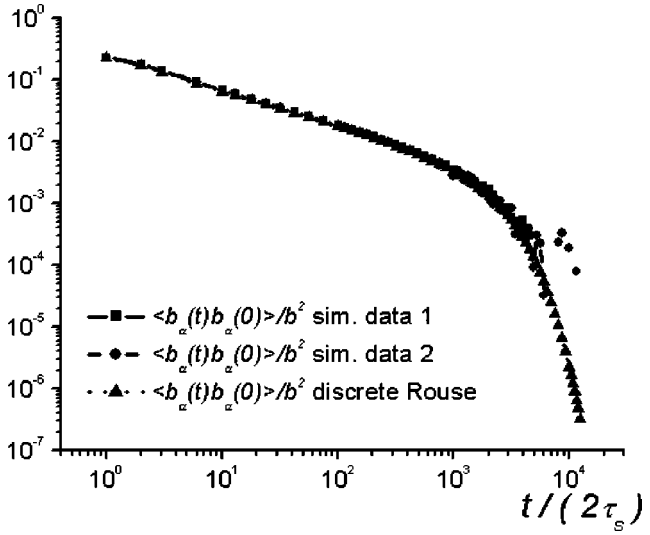

FIG. 6. Test of the modified Stockmayer chain model with a Monte Carlo simulation of the correlation functions of the tangent vector components of an unconfined chain with $N=50$ Kuhn segments of fixed length without excluded-volume interactions. For comparison, theoretical data for the discrete Rouse model were numerically evaluated according Eq. (45). The time unit in this evaluation was set to $2\tau_s$. In the Monte Carlo simulation, N random rotations per chain and time unit were allowed for. Data sets of two independent simulations are plotted.

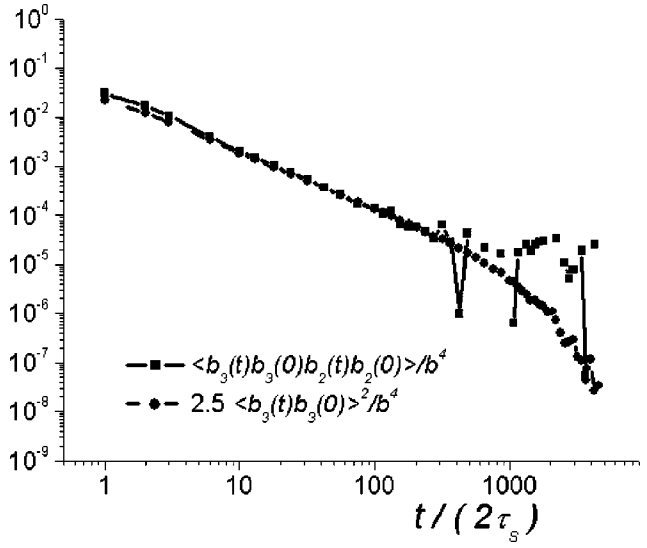

FIG. 7. Test of the modified Stockmayer chain model with a Monte Carlo simulation of the functions $2.5\langle b_3(t)b_3(0)\rangle^2$ and $\langle b_3(t)b_3(0)b_2(t)b_2(0)\rangle$ [see Eqs. (20)–(22)] of an unconfined chain with $N=50$ Kuhn segments of fixed length without excluded-volume interactions. The time unit was set to $2\tau_s$ corresponding to N random rotations per chain. The two functions tend to coincide for $t \gg \tau_s$ as predicted by the theory for the discrete Rouse model.

and the tangent vector component correlation function, respectively.

A further test is based on Eqs. (20)–(22), which suggest that $\langle b_3(t)b_3(0)b_2(t)b_2(0)\rangle$ should become equal to $2.5\langle b_3(t)b_3(0)\rangle^2$ in the long-time limit $t \gg \tau_s$. Our Monte Carlo simulations again reproduce this crucial theoretical prediction reliably as demonstrated in Fig. 7.

Monte Carlo simulations based on the modified Stockmayer chain model also verify Eq. (2) for the spin-lattice relaxation dispersion of a free Rouse chain. Figure 8 shows

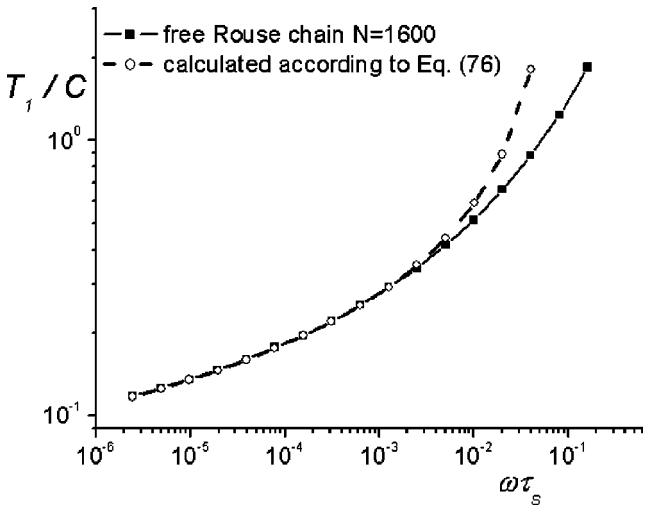

FIG. 8. T_1 dispersion for the free Rouse chain simulated with the modified Stockmayer chain model and calculated according to Eq. (76). The constant C is equal to $(\tilde{M}_2\tau_s)^{-1}$. For $\omega \ll \tau_s^{-1}$ the simulated data and the analytical theory[10–13] coincide perfectly and reproduce the behavior experimentally found for melts of various polymer species below the critical molecular mass (Refs. 8, 12–15).

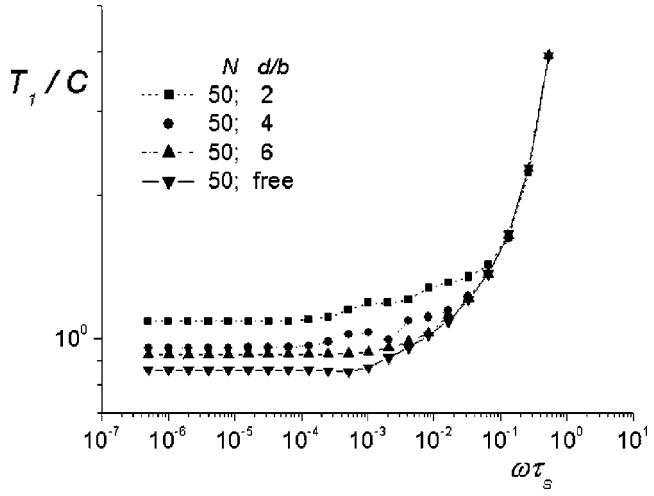

FIG. 9. T_1 dispersion obtained from simulations of a chain ($N=50$) in a straight tube with an infinitely deep square well radial potential for various tube diameters. The constant C is equal to $(\tilde{M}_2\tau_s)^{-1}$. With increasing tube diameter d the free-chain behavior is more and more approached.

the results obtained for chains with $N=1600$ Kuhn segments. In the range $\tau_R^{-1} \ll \omega^{-1} \ll \tau_s^{-1}$ it can perfectly be described by the relation

$$\frac{1}{T_1} = 0.82\,\tilde{M}_2\tau_s \ln\left(\frac{0.23}{\omega\tau_s}\right). \tag{76}$$

This logarithmic frequency dependence complies to the theoretical prediction[10–13] as well as to experimental data acquired with melts of a series of different polymer species below the critical molecular mass.[8,12–15]

C. Monte Carlo simulation of chains confined in an infinitely deep square-well radial potential

The modified Stockmayer chain model was then used to simulate polymer dynamics in an infinitely deep square-well radial potential. According to the common Metropolis algo-

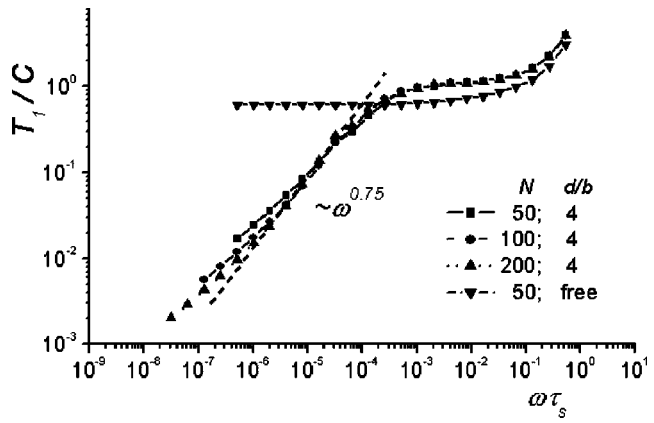

FIG. 10. T_1 dispersion obtained from simulations of chains in a randomly coiled tube with an infinitely deep square well radial potential for various chain lengths. The constant C is equal to $(\tilde{M}_2\tau_s)^{-1}$. The power law $T_1 \propto \omega^{3/4}$ is represented by the dashed line.

rithm, the probability of the chain to cross the tube wall was set to zero. That is, all rotational segment jumps are ignored that would cross the tube wall.

Figure 9 shows the T_1 dispersion for a Rouse chain in a straight tube. With decreasing tube diameter d the frequency dependence becomes more and more flat for $\omega \leqslant 1/\tau_e$. This behavior reflects the reduced variation of the correlation functions of the tangent vector components due to the restrictions in the x,y plane perpendicular to the tube axis.

The low-frequency T_1 dispersion changes if the tube conformation corresponds to a random coil, i.e., has a Gaussian conformation. Segment displacements along the tube axis (i.e., reptation) then lead to further reorientations which reduce the residual correlation remaining in the straight-tube case. This gives rise to the low-frequency dispersion expected according to Eq. (1) for $\omega\tau_e \ll 1$. In this case, the simulated correlation functions were multiplied by $P(\tilde{l};t)$ according to Eqs. (69) and (70), where $\langle \delta x_3^2(t) \rangle$ was taken from the simulations. Figure 10 shows the simulation data obtained for a chain in a randomly coiled tube with an infinitely deep square-well radial potential. The theoretical low-frequency dispersion, as well as the predicted absence of a strong dependence on the chain length, are reproduced with reasonable accuracy.

IX. DISCUSSION

The problem of chain dynamics in a tube has been studied analytically and with the aid of a Monte Carlo computer simulation with respect to spin-lattice relaxation dispersion and the anomalous mean-squared segment displacement behavior. For the analytical treatment cylindrical tubes with a harmonic radial potential were assumed. The crossover from Rouse dynamics of free chains to reptation dynamics in tubes tight enough to impose topological constraints on chain dynamics on the time scale considered has clearly been demonstrated.

The analytical theory is straightforward and qualitatively reproduces predictions for the Rouse model and the ordinary tube/reptation model. This includes the laws for the spin-lattice relaxation time $T_1 = -\beta/\tau_s \ln(\omega\tau_s)$ for $\omega \ll \tau_s^{-1}$ (free Rouse chains) and $T_1 \propto M^0 \omega^{0.75}$ for $\tau_e^{-1} \ll \omega \ll \tau_R^{-1}$ (reptation in a randomly coiled tube). Note that none of these laws implies any dependence on the molecular mass.

Both laws were already verified in experimental NMR studies. Employing field-cycling NMR relaxometry, the T_1 dispersion of polymer melts below the critical molecular mass was shown to obey the logarithmic law characteristic for Rouse dynamics.[8,12–15] On the other hand, the peculiar frequency dependence predicted for reptation in the range given above was identified with polymers topologically constrained by artificial nanotubes in a solid matrix.[3–5]

The analytical theory for polymers confined in randomly coiled pores with harmonic radial potentials in the tubes leads to the anomalous mean-squared segment displacement laws $\langle r^2 \rangle \propto M^0 t^{1/2}$ for $\tau_s \ll t \ll \tau_e$, $\langle r^2 \rangle \propto M^0 t^{1/4}$ for $\tau_e \ll t \ll \tau_R$, and $\langle r^2 \rangle \propto M^{-1/2} t^{1/2}$ for $t \gg \tau_R$ which coincides with predictions of the ordinary tube/reptation model. The latter law was also verified experimentally in our previous fringe field NMR diffusometry study of polymers confined in nanopores of a rigid matrix.[3,5]

Note that no such combined molecular weight and time or frequency dependences mentioned so far were ever found in NMR experiments with free melts of entangled polymers although the field-cycling NMR relaxometry technique[9] is a particularly powerful tool for probing chain modes in just the dynamic range of interest. The conclusion is that the static nature of the tube as it was anticipated in the present treatment as well as in the experiments referred to appears to be a crucial prerequisite for reptation dynamics in the strict sense. Chain dynamics in melts of entangled polymers obviously tend to be more isotropic than postulated by the tube/reptation model. That is, the effective tube diameter is not stationary but increases with time, at least in the range 10^{-8} to 10^{-2} s. The ingenious simplicity and internal harmony of the tube/reptation concept must, thus, be sacrificed to a certain degree. It remains to modern liquid state theory to develop statistical physics approaches leading to a better understanding of experimental facts in this context. A discussion and review of this field is however beyond the scope of the present paper.

Chain dynamics in tubes has also been examined with the aid of Monte Carlo simulations. For this purpose, the Stockmayer chain model was modified in order to achieve consistent results. Test runs with unconfined chains perfectly reproduced the well-known characteristics of Rouse dynamics. The simulation method is therefore considered to be particularly reliable.

In this Monte Carlo study we examined chain dynamics in straight and randomly coiled cylindrical tubes with an infinitely deep square-well radial potential. The tube diameter was varied. The primary quantities to be evaluated in the simulations are the mean-squared segment displacement and correlation functions of components of the segment tangent vector. We have in particular focused on the latter in order to derive the frequency dependence of the spin-lattice relaxation time T_1 via the Fourier transform expression given in Eq. (60).

The numerically simulated results for infinitely deep square-well radial potentials (''hard tubes'') and the analytically derived data for harmonic radial potentials (''soft tubes'') were found to be qualitatively the same. Two T_1 dispersion regimes can be distinguished for randomly coiled tubes. In the upper frequency range of our study, local segment reorientation are dominating and the T_1 dispersion deviates little from that of free chains. An important feature of this high-frequency process is that it connected with a certain residual correlation that does not decay to zero unless some additional reorientation mechanism comes into play (for a discussion see also Ref. 8) This is in contrast to the low-frequency range, where the coiled tube conformation is probed by reptational displacements leading to additional segment reorientations, which make orientation correlations vanish in the limit of long times.

Between these two mechanisms, a plateau-like region shows up, especially if the effective tube diameters d approaches the Flory random coil diameter of the chain. The low-frequency T_1 dispersion due to reptational segment dis-

placements is characterized by a strong frequency dependence which asymptotically approaches

$$\frac{1}{T_1}=\frac{2\Gamma(\frac{5}{4})}{15}\{1+2\cdot 2^{1/4}\}\frac{\tilde{M}_2\tau_s}{(\omega\tau_s)^{3/4}}\frac{1}{b^4}\{\langle b_1^2(0)\rangle-\langle b_3^2(0)\rangle\}^2. \tag{77}$$

In the case of soft tubes the crossover to the $\omega^{3/4}$ dispersion is less abrupt than with hard tubes. Anyway, and remarkably, it shows up already with a ratio between the effective tube diameter and the Flory radius of $R_F/d\simeq 8$ is already clearly visible (see Fig. 2). That is, there is a strong effect of the tube potential on chain dynamics even on a length scale close to the characteristic random coil parameters of the polymer. On the other hand, relatively little influence can be stated with respect to excluded-volume interactions which merely make "soft tube" dynamics more similar to "hard tube" behavior.

ACKNOWLEDGMENTS

This work was supported by the Volkswagen Stiftung, CRDF, and INTAS.

APPENDIX: DERIVATION OF EQUATIONS (62) AND (63)

The Cartesian components of the tangent vector $b_n^e(t)$ in laboratory frame, $e=x,y,z$ are to be expressed by Cartesian components $b_{\alpha n}(t)$ in a coordinate system with the axes x_1,x_2,x_3. The angle between the axes z and x_3 is denoted by θ. The coordinates x_1 and x_2 are identical because of the axial symmetry of the potential $U(\rho)$. The axis y can therefore be chosen parallel to x_2 and we have

$$\begin{aligned} x&=x_1\cos\theta-x_3\sin\theta,\\ y&=x_2,\\ z&=x_1\sin\theta+x_3\cos\theta. \end{aligned} \tag{78}$$

Elementary calculations lead to the following results:

$$\begin{aligned} &\langle b^z(t)b^z(0)b^+(t)b^-(0)\rangle\\ &\quad=\cos^2\theta\sin^2\theta\{\langle b_1^2(t)b_1^2(0)\rangle\\ &\qquad+\langle b_3^2(t)b_3^2(0)\rangle-2\langle b_1^2(0)\rangle\langle b_3^2(0)\rangle\}\\ &\qquad+(\sin^4\theta+\cos^4\theta-2\sin^2\theta\cos^2\theta)\\ &\qquad\times\langle b_1(t)b_3(t)b_3(0)b_1(0)\rangle\\ &\qquad+\sin^2\theta\langle b_1(t)b_2(t)b_2(0)b_1(0)\rangle\\ &\qquad+\cos^2\theta\langle b_3(t)b_2(t)b_2(0)b_3(0)\rangle \end{aligned} \tag{79}$$

and

$$\begin{aligned} &\langle(b_n^+(t))^2(b_n^-(0))^2\rangle\\ &\quad=\cos^4\theta\langle b_1^2(t)b_1^2(0)\rangle\\ &\qquad+\langle b_2^2(t)b_2^2(0)\rangle+\sin^4\theta\langle b_3^2(t)b_3^2(0)\rangle\\ &\qquad+4\cos^2\theta\langle b_1(t)b_2(t)b_2(0)b_1(0)\rangle\\ &\qquad+4\sin^2\theta\cos^2\theta\langle b_1(t)b_3(t)b_3(0)b_1(0)\rangle\\ &\qquad+2\sin^2\theta\cos^2\theta\langle b_1^2(0)\rangle\langle b_3^2(0)\rangle\\ &\qquad+4\sin^2\theta\langle b_2(t)b_3(t)b_3(0)b_2(0)\rangle\\ &\qquad-2\cos^2\theta\langle b_1^2(0)\rangle\langle b_2^2(0)\rangle-2\sin^2\theta\langle b_2^2(0)\rangle\langle b_3^2(0)\rangle. \end{aligned} \tag{80}$$

Segment displacements in directions x_1, x_2, and x_3 in accordance with Eq. (22) are independent of each other. The stochastic Langevin force $\mathbf{f}_{nL}(t)$ is a normal Gaussian stochastic process. One can therefore employ the following decoupling relations

$$\begin{aligned} &\langle b_\alpha^2(t)b_\alpha^2(0)\rangle=\langle b_\alpha^2(0)\rangle^2+2\langle b_\alpha(t)b_\alpha(0)\rangle^2,\\ &\langle b_\alpha(t)b_\beta(t)b_\alpha(0)b_\beta(0)\rangle\\ &\quad=\langle b_\alpha(t)b_\alpha(0)\rangle\langle b_\beta(t)b_\beta(0)\rangle,\quad \text{for } \alpha\neq\beta\\ &\langle b_\alpha^2(t)b_\beta^2(0)\rangle=\langle b_\alpha^2(0)\rangle\langle b_\beta^2(0)\rangle \end{aligned} \tag{81}$$

and, because the axes x_1 and x_2 are equivalent,

$$\langle b_1^2(0)\rangle=\langle b_2^2(0)\rangle. \tag{82}$$

Inserting Eqs. (81) and (82) in Eqs. (79) and (80), and averaging over all possible values of θ, leads to

$$\begin{aligned} &\langle b^z(t)b^z(0)b^+(t)b^-(0)\rangle\\ &\quad=\tfrac{14}{15}\langle b_1(t)b_1(0)\rangle^2+\tfrac{4}{5}\langle b_1(t)b_1(0)\rangle\langle b_3(t)b_3(0)\rangle\\ &\qquad+\tfrac{4}{15}\langle b_3(t)b_3(0)\rangle^2+\tfrac{2}{15}\{\langle b_1^2(0)\rangle^2-\langle b_3^2(0)\rangle^2\}^2 \end{aligned} \tag{83}$$

and

$$\begin{aligned} &\langle(b_n^+(t))^2(b_n^-(0))^2\rangle\\ &\quad=\tfrac{56}{15}\langle b_1(t)b_1(0)\rangle^2+\tfrac{16}{5}\langle b_1(t)b_1(0)\rangle\langle b_3(t)b_3(0)\rangle\\ &\qquad+\tfrac{16}{15}\langle b_3(t)b_3(0)\rangle^2+\tfrac{8}{15}\{\langle b_1^2(0)\rangle^2-\langle b_3^2(0)\rangle^2\}^2. \end{aligned} \tag{84}$$

In the isotropic case (free Rouse chains) we have $\langle b_\alpha(t)b_\alpha(0)\rangle=\frac{1}{3}\langle\mathbf{b}(t)\mathbf{b}(0)\rangle$ for all $\alpha=1,2,3$. Equations (83) and (84) then become

$$\langle b^z(t)b^z(0)b^+(t)b^-(0)\rangle=\tfrac{2}{9}\langle\mathbf{b}(t)\mathbf{b}(0)\rangle_0^2 \tag{85}$$

and

$$\langle(b_n^+(t))^2(b_n^-(0))^2\rangle=\tfrac{8}{9}\langle\mathbf{b}(t)\mathbf{b}(0)\rangle_0^2. \tag{86}$$

[1] P. G. de Gennes, J. Chem. Phys. **55**, 572 (1971).
[2] M. Doi and S. F. Edwards, *The Theory of Polymer Dynamics* (Clarendon, Oxford, 1986).
[3] E. Fischer, R. Kimmich, U. Beginn, M. Möller, and N. Fatkullin, Phys. Rev. E **59**, 4079 (1994).
[4] R. Kimmich, R.-O. Seitter, U. Beginn, M. Möller, and N. Fatkullin, Chem. Phys. Lett. **307**, 147 (1999).
[5] R. Kimmich, N. Fatkullin, R.-O. Seitter, E. Fischer, U. Beginn, and M. Möller, Macromol. Symp. **146**, 109 (1999).
[6] U. Beginn, E. Fischer, T. Pieper, F. Mellinger, R. Kimmich, and M. Möller, J. Polym. Sci., Part A: Polym. Chem. **38**, 2041 (2000).
[7] R. Kimmich, N. Fatkullin, R.-O. Seitter, and K. Gille, J. Chem. Phys. **108**, 2173 (1998).
[8] R. Kimmich, N. Fatkullin, H. W. Weber, and S. Stapf, J. Non-Cryst. Solids **172–174**, 689 (1994).
[9] R. Kimmich, *NMR Tomography, Diffusometry and Relaxometry* (Springer, Berlin, 1997).
[10] T. N. Khazanovich, Polym. Sci. U.S.S.R. **4**, 727 (1963).

[11] R. Ullman, J. Chem. Phys. **4**, 1558 (1966).
[12] N. Fatkullin, R. Kimmich, and H. W. Weber, Phys. Rev. E **47**, 4600 (1993).
[13] N. Fatkullin and R. Kimmich, J. Chem. Phys. **101**, 822 (1994).
[14] H. W. Weber and R. Kimmich, Macromolecules **26**, 2597 (1993).
[15] R. Kimmich and H. W. Weber, J. Chem. Phys. **98**, 5847 (1993).
[16] V. Yamakov, D. Stauffer, A. Milchev, G. M. Foo, and R. B. Pandey, Phys. Rev. Lett. **79**, 2356 (1997).
[17] F. Zhang, J. Chem. Phys. **111**, 9082 (1999).
[18] P. Sotta, A. Lesne, and J. M. Victor, J. Chem. Phys. **113**, 6966 (2000); **112**, 1565 (2000).
[19] Yu-Jane Sheng and Meng-Chien Wang, J. Chem. Phys. **114**, 4724 (2001).
[20] P. H. Verdier and W. H. Stockmayer, J. Chem. Phys. **36**, 227 (1962).
[21] A. Yu. Groswert and A. R. Khokhlov, *Statistical Physics of Macromolecules* (AIP, New York, 1994).
[22] A. Abragam, *The Principles of Nuclear Magnetism* (Clarendon, Oxford, 1961).
[23] M. F. Herman, J. Chem. Phys. **112**, 3040 (2000).
[24] M. E. J. Newman and G. T. Barkema, *Monte Carlo Methods in Statistical Physics* (Clarendon, Oxford, 1999).
[25] A. Perico and M. J. Guenza, J. Chem. Phys. **83**, 3103 (1985).